Journal of Medicinal Chemistry

Article

pubs.acs.org/jmc

Unprecedented Binding Mode of Hydroxamate-Based Inhibitors of Glutamate Carboxypeptidase II: Structural Characterization and Biological Activity

Zora Novakova,[†] Krystyna Wozniak,[‡] Andrej Jancarik,[#] Rana Rais,[‡,§] Ying Wu,[‡] Jiri Pavlicek,[†] Dana Ferraris,[¶] Barbora Havlinova,[†] Jakub Ptacek,[†] Jan Vavra,[#] Niyada Hin,[‡] Camilo Rojas,[‡] Pavel Majer,[#] Barbara S. Slusher,[*,‡,§,∥,⊥] Takashi Tsukamoto,[*,‡,§] and Cyril Barinka[*,†]

[†]Institute of Biotechnology, Academy of Sciences of the Czech Republic, BIOCEV, Prumyslova 595, 252 50 Vestec, Czech Republic

[‡]Johns Hopkins Drug Discovery Program, [§]Departments of Neurology, [∥]Psychiatry and Behavioral Sciences, and [⊥]Neuroscience, Johns Hopkins University, Baltimore, Maryland 21205, United States

[#]Institute of Organic Chemistry and Biochemistry, Academy of Sciences of the Czech Republic, v.v.i., Flemingovo n. 2, 166 10 Prague 6, Czech Republic

[¶]Department of Chemistry, McDaniel College, 2 College Hill, Westminster, Maryland 21157, United States

Supporting Information

ABSTRACT: Inhibition of glutamate carboxypeptidase II (GCPII) is effective in preclinical models of neurological disorders associated with excessive activation of glutamatergic systems. Here we report synthesis, structural characterization, and biological activity of new hydroxamic acid-based inhibitors with nanomolar affinity for human GCPII. Crystal structures of GCPII/hydroxamate complexes revealed an unprecedented binding mode in which the putative P1′ glutarate occupies the spacious entrance funnel rather than the conserved glutamate-binding S1′ pocket. This unique binding mode provides a mechanistic explanation for the structure−activity relationship data, most notably the lack of enantiospecificity and the tolerance for bulky/hydrophobic functions as substituents of a canonical glutarate moiety. The in vivo pharmacokinetics profile of one of the inhibitors will be presented along with analgesic efficacy data from the rat chronic constrictive injury model of neuropathic pain.

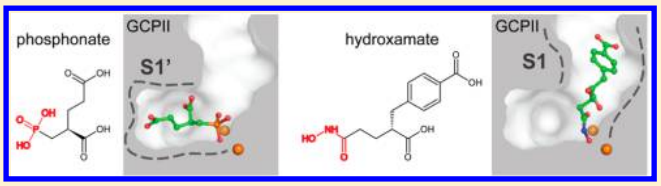

INTRODUCTION

Glutamate carboxypetidase II (GCPII; EC 3.4.17.21), also known as *N*-acetylated-α-linked acidic dipeptidase (NAALADase), is a membrane-bound zinc-dependent metallopeptidase that has been exploited as a therapeutic target of a variety of neurological disorders as well as a marker for prostate cancer imaging.[1] Within the central/peripheral nervous system, astrocyte/Schwann cell-bound GCPII is primarily responsible for the hydrolysis of *N*-acetylaspartylglutamate (NAAG), the most prevalent and widely distributed mammalian neuropeptide.[2−4] Catabolism of extracellular NAAG yields *N*-acetylaspartate and glutamate. Under pathologic conditions, excessive glutamate generated by GCPII can lead to neuronal dysfunction and degeneration through overactivation of the glutamatergic neurotransmission systems. Taking into account the concomitant neuroprotective role of NAAG,[5,6] it is assumed that the inhibition of GCPII can attenuate neurotoxicity associated with enhanced glutamate transmission. Indeed, GCPII inhibitors demonstrate efficacy in multiple preclinical models including traumatic brain injury, stroke, amyotrophic lateral sclerosis, and neuropathic and inflammatory pain.[7−11]

Prior structural studies offered a detailed insight into the overall GCPII architecture that could be used for the structure-assisted design of GCPII-specific compounds (reviewed by Pavlicek et al).[12] The S1′ pocket is the principal site targeted by GCPII inhibitors, and it shows very strong preference for glutamate and glutamate mimics that are the hallmark of the overwhelming majority of GCPII binders.[13,14] Contrary to the profound selectivity of the S1′ pocket, the spacious and structurally ill-defined nonprime site(s), which are continuous with the entrance funnel, can accommodate a variety of moieties of diverse sizes and physicochemical characteristics.[15]

The pharmacophore of GCPII inhibitors consists of a zinc-binding group (ZBG) linked to a P1′ glutamate-based moiety that is designed to interact with the active-site zinc ions and residues shaping the S1′ pocket, respectively (Figure 1a).[13,14] The most prominent ZBGs used in the design of GCPII inhibitors include ureas and phosphorus-based (phosphinates, phosphonates, and phosphoramidates) functions, for which a wealth of structural, SAR, and biological data has been reported in the literature.[16−18] Despite this fact, however, neither of the two structural classes was determined to have appreciable oral bioavailability and therefore are not ideal to pursue as

Received: November 19, 2015
Published: April 13, 2016

DOI: 10.1021/acs.jmedchem.5b01806
J. Med. Chem. 2016, 59, 4539−4550

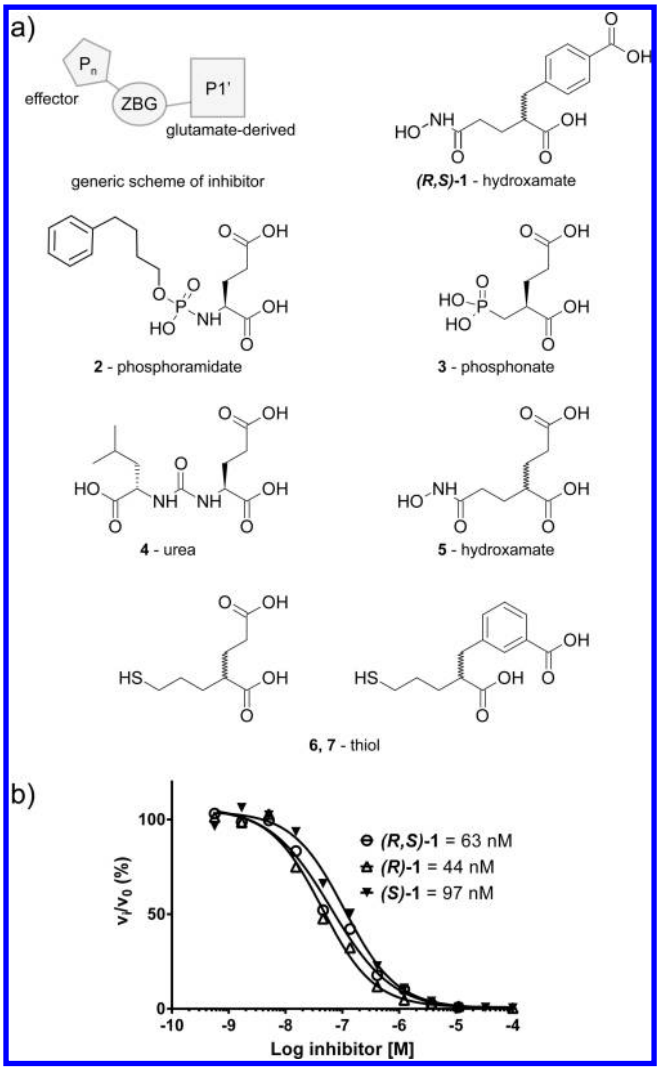

Figure 1. Formulas and inhibitory profiles of GCPII inhibitors. (a) Formula of a generic GCPII inhibitor and examples of GCPII inhibitors with various ZBGs used in the field. A zinc-binding group (ZBG) is attached to a P1′ substituent function (typically glutarate) via a flexible linker forming together a GCPII-specific pharmacophore module. Nonprime (effector) functionality extends into the spacious internal funnel, modulates physicochemical and inhibitory characteristics of GCPII binders, and imparts required functional properties for biological applications. Inhibitors used in the field: **2**, MP1D; **3**, 2-PMPA; **4**, ZJ-43; **6**, 2-MPPA. (b) Inhibition curves determined by the radioenzymatic assay. Corresponding IC_{50} values are 44, 97, and 63 nM for (*R*)-**1**, (*S*)-**1**, and (*R*,*S*)-**1**, respectively.

therapeutics for a chronic disease. To diversify a portfolio of ZBGs used for targeting GCPII, we and other groups introduced thiols, sulfonamides, and hydroxamates as alternative ZBGs (Figure 1a).[19−21]

The present study specifically focuses our ZBG diversification strategy on hydroxamic acids, one of the most prominent ZBGs used in the design of metallohydrolase inhibitors. Hydroxamate function is favored for its strong chelating properties of metal ions, including active site-bound zinc and nickel cations. Hydroxamate-based inhibitors were successfully used to inhibit urease, carbonic anhydrase, and matrix metalloproteases.[22,23] Additionally, Vorinostat, a broad spectrum hydroxamate-derived inhibitor of histone deacetylases, was FDA-approved for the treatment of cutaneous T cell lymphoma, documenting clinical utility and oral bioavailability of hydroxamates in human medicine.[24] Combined in vitro and in vivo data presented here provide further experimental evidence for oral bioavailability and in vivo efficacy of hydroxamate-based compounds, and the structural findings can be used as an excellent starting point for future SAR studies aimed at the development of the next generation of GCPII-specific compounds.

RESULTS

Hydroxamic Acid-Based Inhibitors. The design of hydroxamic acid-based compounds used in this study follows a general template exploited for known GCPII-specific inhibitors (Figure 1a). Accordingly, the compounds comprise a zinc-binding group (hydroxamic acid) connected to a side chain substituent (benzoate function) via a flexible linker (2-carboxybutyl moiety; compounds (*R*)-**1**, (*S*)-**1**, (*R*,*S*)-**1** Scheme 1). The protected parent racemic mixture **15** was synthesized according to the Scheme 1 in eight linear steps with a 27% overall yield. The individual enantiomers of **15** were isolated using a Eurocel 01 column in a linear gradient of *n*-heptane/ethanol (2:1; Supporting Information Figure S1). Isolated optical isomers, together with the parent racemic mixture, were deprotected using hydrogenation to yield compounds (*R*)-**1**, (*S*)-**1**, and (*R*,*S*)-**1**, respectively. The identity of all intermediates compounds were confirmed by HR-MS, ^{1}H NMR, ^{13}C NMR, analytical HPLC, and optical rotation where appropriate. The optical purity was determined by analytical HPLC on the Eurocel 01 column and optical rotation measurements revealed $[\alpha]^{22}_{D}$ +10.7°and $[\alpha]^{22}_{D}$ −10.0°, for (*R*)-**1** and (*S*)-**1**, respectively. The absolute configuration of (*R*)-**1** and (*S*)-**1** at the asymmetric carbon was not known at the time of synthesis but was later assigned from the electron density maps of GCPII/inhibitor X-ray structures (see below).

To assess inhibitory properties as well as the importance of the stereochemistry at the chiral center, we determined inhibition constants in a standard assay setup using radiolabeled [^{3}H]-NAAG as a substrate. Our data revealed IC_{50} values of 44, 97, and 63 nM for (*R*)-**1**, (*S*)-**1**, and (*R*,*S*)-**1**, respectively (Figure 1b). Observed nanomolar inhibition constants are lower compared even to the most potent compound from a series of hydroxamates having the "canonical" P1′ glutamate side chain substituent that has been reported previously (compound **5** IC_{50} = 1200 nM).[20] These SAR findings are surprising when related to the phosphorus and urea-based inhibitors, where the replacement of the canonical P1′ glutamate inevitably led to the decrease in inhibitor potency.[25−27] Furthermore, the enantiomers (*R*)-**1** and (*S*)-**1** are nearly equipotent against GCPII, which goes against the typical GCPII stereoselectivity for known substrates and inhibitors (with the notable exception of thiol-based compounds).

The Bimetallic Active Site Arrangement. The lack of enantiospecificity implies that the binding mode of hydroxamates may differ from binding modes of other structural classes of GCPII inhibitors, structures of which were reported previously.[12] To rationalize this finding as well as to provide a starting point for our future SAR campaign(s), we determined crystal structures of GCPII complexes with (*R*)-**1** and (*S*)-**1** at the high resolution limits of 1.81 and 1.80 Å, respectively. For both complexes, the strong positive electron density representing the active site-bound ligand was observed and individual

DOI: 10.1021/acs.jmedchem.5b01806
J. Med. Chem. 2016, 59, 4539−4550

Scheme 1[a]

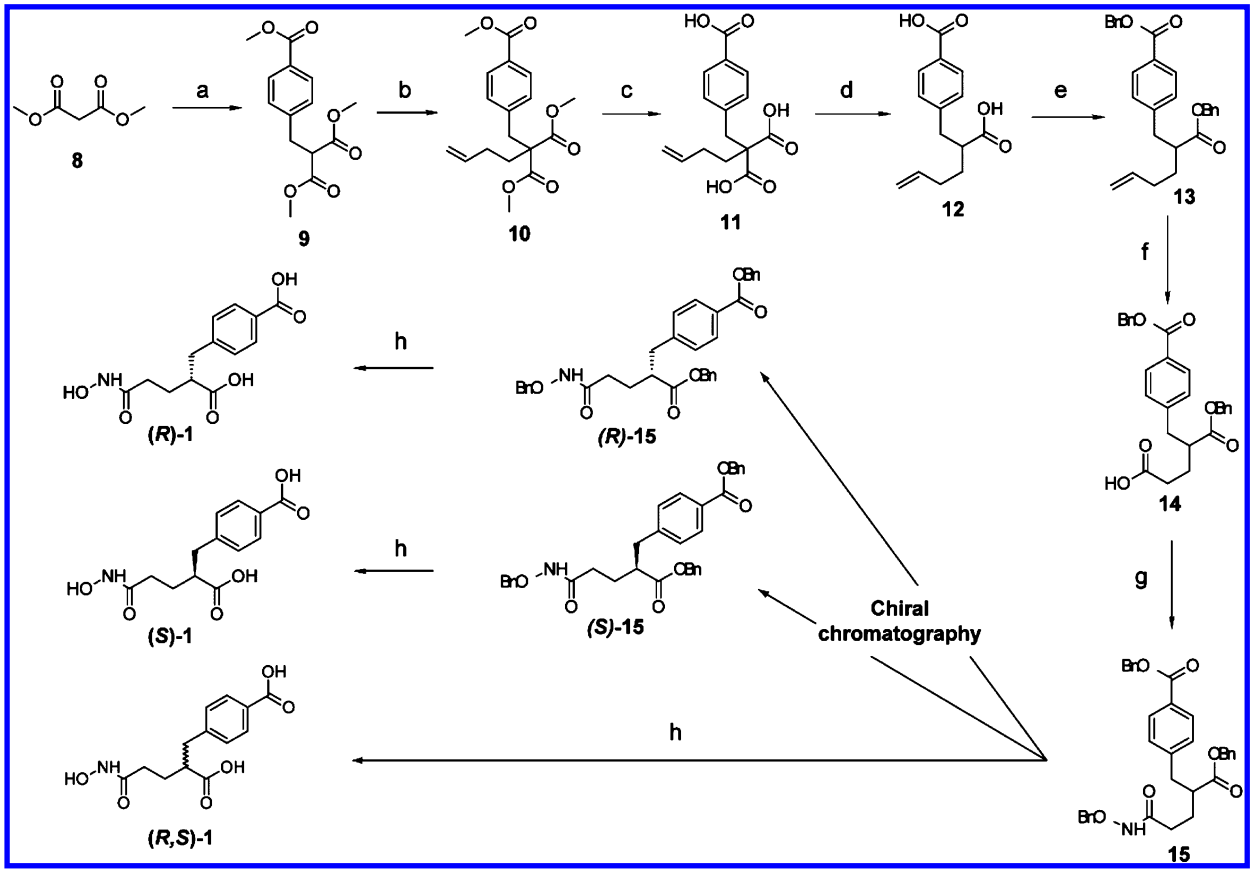

[a]Reagents: (a) NaH, methyl 4-(bromomethyl)benzoate, THF, rt, 12 h, 84%; (b) NaH, 4-bromobut-1-ene, THF, reflux, 4 days, 64%; (c) NaOH (aq), reflux, 24 h, 90%; (d) DMF, 130 °C, 4 h, 88%; (e) BnBr, K_2CO_3, DMF, 80 °C, 24 h, 99%; (f) CH_3CN/H_2O, RuO_2, $NaIO_4$, 0°C to rt, 14 h, 95%; (g) *O*-benzyl hydroxylamine, EDC, DMAP, DCM, rt, 18 h, 68%; (h) H_2/Pd/C, THF, rt, 12 h, 98%.

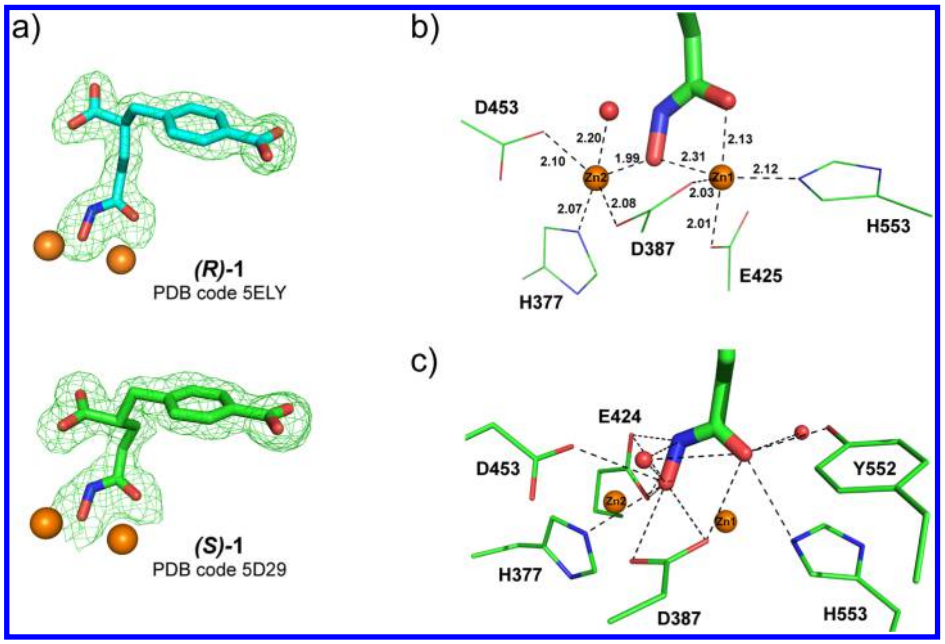

Figure 2. Structural characterization of GCPII/hydroxamate complexes. (a) $F_o - F_c$ maps (green) for (*R*)-**1** and (*S*)-**1**, respectively, are contoured at 3.0 σ, and modeled inhibitors are shown in stick representation with atoms colored cyan and green (carbons of (*R*)-**1** and (*S*)-**1**, respectively), red (oxygen), and blue (nitrogen). The active-site zinc ions are shown as orange spheres. (b) Details of the coordination sphere of the bimetallic dizinc center of GCPII. The inhibitor is shown in stick representation and GCPII residues completing zinc coordination sphere as lines. Distances are in Å. (c) Details of hydrogen bonding interactions of the hydroxamic acid headgroup with GCPII residues. H-bonds shorter than 3.5 Å are shown as broken lines.

DOI: 10.1021/acs.jmedchem.5b01806
J. Med. Chem. 2016, 59, 4539−4550

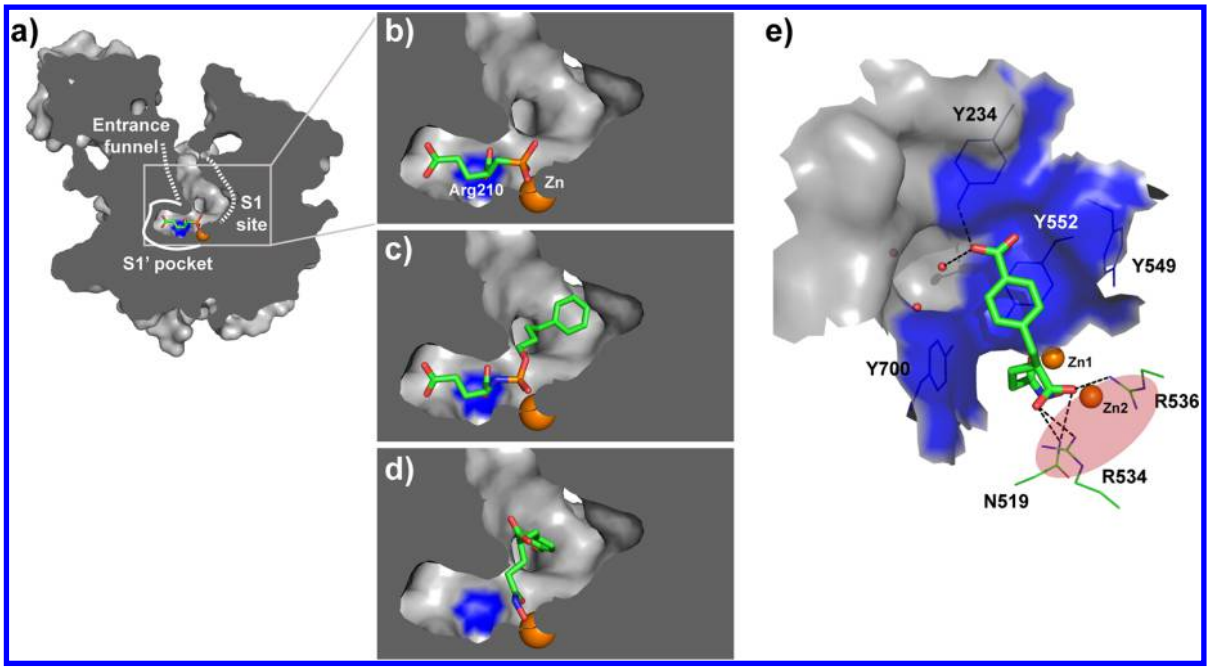

Figure 3. Atypical positioning of (*R*)-**1** in the internal cavity of GCPII. (a) Cross-section of GCPII showing internal inhibitor binding cavity comprising the glutamate-specific S1′ site and the nonprime spacious entrance funnel including the S1 site. Close-up of the internal cavity showing binding modes of **3** (b), **2** (c), and (*R*)-**1** (d). Notice the atypical positioning of the substituent function of (*R*)-**1** that is oriented into the entrance funnel of GCPII. To the contrary, the P1′ glutarate of **2** and **3** is placed into the S1′ (glutamate-binding) pocket of the enzyme. Zinc ions are shown as orange spheres and Arg210 (contributing to the GCPII enantioselectivity toward L-configuration at the P1′ position of a given inhibitor) is colored blue. (e) Tyrosine-rich pocket of GCPII. The distal benzoate group of (*S*)-**1** (in stick representation) occupies a hydrophobic pocket formed by side chains of Tyr549, Tyr552, and Tyr700 (shown as a combination of semitransparent surface and lines; colored blue). The distal carboxylate forms H-bonds with Tyr234 and a water molecule and the P1 α-carboxylate interacts with residues, forming the arginine patch (red semitransparent oval; hydrogen bonds shown as broken lines). Active-site zinc ions are shown as orange spheres.

compounds were fitted into the positive peaks of the $F_o - F_c$ density map in the final stages of the refinement (Figure 2a).

The inspection of bimetallic active site reveals a distorted trigonal−bipyramidal geometry around both the catalytic (Zn1) and cocatalytic (Zn2) zinc ions with the hydroxamic acid group filling three of these positions. The amidohydroxamate group bridges the two zinc ions in an asymmetric fashion with interatomic distances 1.99 and 2.31 Å, while the carbonyl oxygen completes the coordination sphere of Zn1 in the distance of 2.13 Å. The hydroxamate function thus binds Zn1 in a bidentate fashion, while Zn2 is engaged monodentately (Figure 2b).

In addition to the zinc chelation, a multitude of polar interactions between the heteroatoms of the hydroxamic acid functionality and residues forming the active site are observed. The carbonyl oxygen accepts hydrogen bonds from side chains of Asp387 (3.3 Å), Tyr552 (2.6 Å), and His553 (3.0 Å) and participates in water-mediated H-bonds with side chains of Asp453 and Asp387. The hydroxamate −NH− group forms hydrogen bonds with Glu424 carboxylate (2.8 and 3.3 Å), Asp453 (3.4 Å), and a water molecule (3.1 Å) that is in turn H-bonded to Asp453 (2.8 Å) and Asp387 (2.9 and 2.9 Å). Finally, the hydroxyl group of the hydroxamic acid function forms multiple H-bonds with neighboring residues including His377 (3.0 Å), Asp387 (3.3 and 3.3 Å), Glu424 (2.7 and 3.1 Å), and Asp453 (3.2 Å) and a water molecule (2.9 Å; Figure 2c and Supporting Information Figure S2). Overall, the intricate web of interactions of the hydroxamic acid with residues/ions in the active site of GCPII likely produces a new binding mode and influences the position of the aromatic side chain into the S1 pocket rather than the canonical glutamate-binding S1′ site (see below; Supporting Information Figure S3).

New Binding Mode of Side Chain Substituents. Without exception, all inhibitors cocrystallized with GCPII so far occupy the S1′ (glutamate binding) site. The glutarate moiety plays important role in the high-affinity/high-specificity of such inhibitors for GCPII. In this respect, structures reported here represent a groundbreaking finding in the design of GCPII inhibitors as our structures reveal that the side chain substituents of (*R*)-**1** and (*S*)-**1** are bound to the S1 site in the spacious entrance funnel rather than the S1′ glutarate binding site (Figure 3a−d).

The P1 carboxylate functionality, which is attached to the hydroxamic acid head via a propanoyl linker, was originally designed to engage the Arg210 guanidinium group of the S1′ pocket in a fashion mimicking such interactions with the α-carboxylate of glutarate (or glutarate-like) substituents. However, due to the atypical positioning of the side chain substituents of (*R*)-**1** and (*S*)-**1**, the P1 carboxylate primarily interacts with Arg534 of the positively charged arginine patch and the side chain of Asn519. Although roughly overlapping, there are some variations in the interaction pattern of the two P1 carboxylates with GCPII residues as well as two surrounding water molecules that result from the different stereochemistry of (*R*)-**1** and (*S*)-**1** at the chiral carbon atom (Supporting Information Figure S4).

The distal benzoate substituent occupies a hydrophobic pocket formed by side chains of Tyr549, Tyr552, and Tyr700 (Figure 3e). The "parallel displaced" $\pi-\pi$ interactions are observed between the terminal benzoyl group of inhibitors and the hydroxyphenyl ring Tyr552 with the distance of 5.1 Å

DOI: 10.1021/acs.jmedchem.5b01806
J. Med. Chem. 2016, 59, 4539−4550

between the ring centers. Additionally, the "T-shaped" orientation is noticeable in the case of Tyr549 and Tyr700 interactions with the terminal inhibitor benzoyl with the shortest distances of 3.6 and 3.5 Å between the closest carbon vertices of the terminal benzoyl group and hydroxyphenyl rings of Tyr552 and Tyr700, respectively. Contrary to the subtle differences in interactions between the P1 carboxylate function and GCPII residues mentioned above, the hydrogen bonding pattern of the more distal aromatic ring carboxylate is virtually uniform for both compounds as it accepts hydrogen bonds from the hydroxyl group of Tyr234 (2.7 Å) and the main-chain amide of Tyr549 (3.5 Å) and forms a water-mediated contact with Gln254 (3.0 Å).

Pharmacokinetics. To evaluate the exposure and target tissue distribution of (*S*)-**1**, its pharmacokinetic properties were investigated following the single-dose peroral administration at 10 mg/kg in mice and the data are summarized in Figure 4a. Plasma concentration was maximal at 15 min and then decreased over a period of 2 h, while the sciatic nerve concentration was mainly constant during the period studied. The sciatic nerve to plasma ratio based on AUC_{0-2h} was calculated to be about 43%, suggesting good sciatic nerve to plasma tissue penetration index.

Chronic Constrictive Injury Model of Neuropathic Pain. In the final set of experiments, we investigated in vivo efficacy of (*S*)-**1** using a rat chronic constrictive injury model of neuropathic pain. To this end, (*S*)-**1** was dosed to rats with developed chronic constrictive injury daily at 10 mg/kg via oral gavage and hyperalgesia testing performed (dosing initiated 10 days postsurgery) by determining withdrawal latencies in response to a constant thermal stimulus. The compound had a significant effect on prolonging the response time to thermal stimulus on the ligated (injured) side from day 4 of dosing (Figure 4b). Response was measured as a difference in latency of the paw on the sham side to a thermal stimulus versus the ligated side in seconds. This effect persisted through day 15 of dosing, when the experiment was terminated. At the same time, (*S*)-**1** had no significant effect on absolute latency of the sham operated side, suggesting a selective antihyperalgesic effect (Figure 4c).

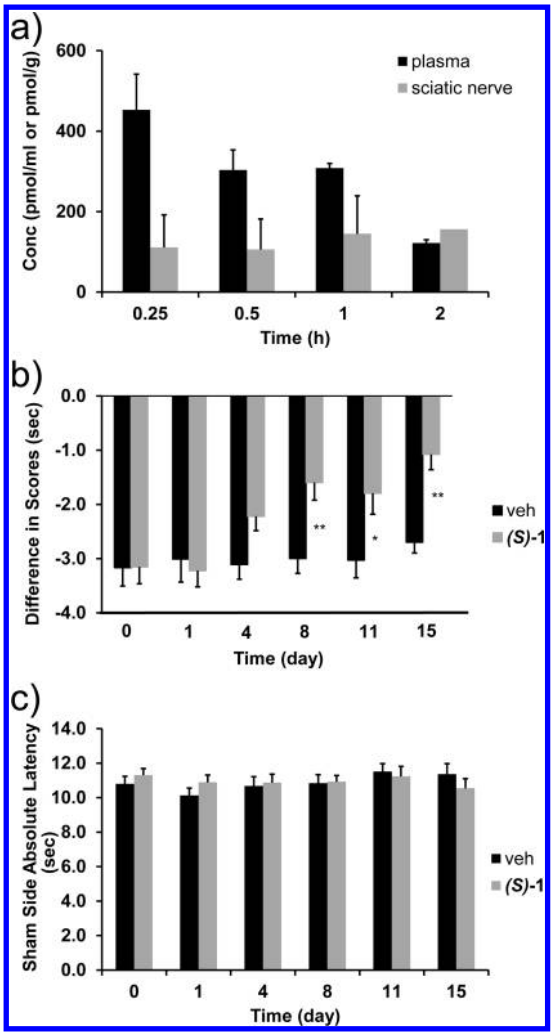

Figure 4. Biological activity of (*S*)-**1**. (a) Pharmacokinetics of (*S*)-**1** in mice (plasma and sciatic nerve concentration) were determined following 10 mg/kg po administration. (b) Analgesic effects of (*S*)-**1** in a rat model of neuropathic pain. The data shown represent the mean difference in paw withdrawal latencies to a thermal stimulus, noted as "Difference in Scores" as determined by subtracting the mean nonligated paw latency from ligated paw response in seconds at baseline (pretreatment) and at various days versus following compound (*S*)-**1** treatment of 10 mg/kg/day po or vehicle. (N = 10 rats per dose group). (c) Compound (*S*)-**1** at 10 mg/kg po had no significant effect on absolute latency of sham operated side. (* denotes $p < 0.05$, ** denotes $p < 0.01$).

DISCUSSION

As the key aspect of this work, we present new hydroxamate-based inhibitors with nanomolar affinity for human GCPII. Using a rat model of neuropathic pain, we demonstrate that this class of compounds is orally active for the treatment of neuropathic pain. The design of compounds (*R*)-**1** and (*S*)-**1** was based on our previous research on thiol-based inhibitors.[19,28] Compounds such as thiol **7** revealed a tolerance for P1′ glutamate substitutions by more lipophilic functions expanding the searchable chemical space and allowing for the synthesis of inhibitors with clogD values more suitable for targeting neurological disorders. The surprising tolerance for a P1′ replacement is fully explained by our structural data showing that the side chains of both hydroxamates (*R*)-**1** and (*S*)-**1** are located in the spacious internal funnel of the enzyme, providing ample space for the incorporation of larger substituents within the inhibitor backbone. Our data thus offer a solid foundation for the structure-assisted development of the next generation hydroxamate-based inhibitors.

The S1′ Pocket and Glutamate Preferences. The amphipathic S1′ pocket of GCPII is located at the very bottom of the substrate-binding internal cavity (Figure 3a). The pocket is highly specific for glutamate and glutamate-like moieties. In general, the profound glutamate selectivity of the S1′ site stems from the combination of several structural features including (i) small dimensions, (ii) limited overall flexibility, (iii) strong ion-pairing between glutamate α-carboxylate/γ-carboxylate and side chains of Arg210 and Lys699, respectively, and (iv) additional intricate network of polar interactions between the enzyme and an inhibitor. The majority of GCPII inhibitors feature glutamate or a glutamate-like function at the P1′ position and substituting the P1′ glutamate of an inhibitor markedly decreases its potency.[15,25,29−31] For example, glutamate substitutions of the parent urea-based DCIBzL inhibitor (IC_{50} = 60 pM) resulted in more than 100-fold decrease in affinity for the enzyme.[27] Similarly, SAR studies on phospho(i)nate-based compounds show a strong preference for the P1′ glutamate

DOI: 10.1021/acs.jmedchem.5b01806
J. Med. Chem. 2016, 59, 4539−4550

over any of derivatives tested, with the 2-PMPA being the prime example of the high-affinity, high-specificity GCPII inhibitor with IC_{50} = 300 pM.[16,25]

Our original study reporting the synthesis of aliphatic hydroxamate-based GCPII inhibitors was based on the assumption that their glutamate is engaged with the interaction with the S1′ pocket of GCPII. The crystal structures of GCPII in complex with the second generation hydroxamate-based inhibitors presented here, however, refute the notion of "indispensability of glutamate" for the design of GCPII inhibitors. Our data represent the first (structural) example of GCPII inhibitors that do not engage with the S1′ glutamate-recognition pocket of GCPII. Although speculative, it is conceivable that aliphatic hydroxamates (and corresponding thiols such as compounds **6** and **7** (Figure 1a)) also bind to GCPII without occupying the S1′ glutamate-recognition pocket. Addressing these questions is important for further SAR research in this direction, which is a focus of our ongoing studies.

GCPII/Inhibitor Interactions in the Entrance Funnel and the S1 Pocket. The nonprime side of the GCPII internal pocket can be viewed as an irregularly shaped water-filled funnel with a wide-opening at the surface of the protein narrowing to the active site-bound zinc ions approximately 20 Å below. The walls of the funnel are mostly of polar residues dotted by several isolated hydrophobic patches formed by side chains of tyrosine residues. Consequently, any inhibitor/substrate entering the internal cavity of the enzyme encounters mainly hydrophilic milieu before being docked and oriented to the active-site and S1/S1′ specificity pockets.

There is a limited positional variability observed for the side chains lining the nonprime side of the GCPII internal pocket but for two notable exceptions. First, the internal pocket can be shielded from the external space by the entrance lid: a flexible loop comprising amino acids Trp541-Gly548. The flexibility, i.e., opening/closing of the entrance lid is likely required for the physiological functioning of the enzyme. Furthermore, so-called arene-binding site, which is a part of the entrance lid, can be exploited for the design of GCPII inhibitors with high affinity and increased selectivity for the GCPII paralogue (see below).[30,32,33] The positively charged arginine patch comprised of Arg463, Arg534, and Arg536 side chains represents the second structural feature in the internal pocket, of which positional flexibility can be exploited for the inhibitor design. We have shown that repositioning of side chains of Arg463 and Arg536 opens a cryptic "S1 accessory pocket" that can accommodate hydrophobic functionalities (such as a phenyl group), contributing thus to increase in inhibitor affinity due to the avidity effect.[29]

Structures presented herein did not reveal any conformational changes in the S1 pocket of GCPII that would be required to accommodate (*R*,*S*)-**1**. In fact, the distal benzoate substituent fits neatly into a "preformed" hydrophobic register defined by Tyr549, Tyr552, and Tyr700 side chains. At the same time, positioning of the hydroxamates solely into the structurally ill-defined nonprimed section of the internal pocket offers a unique opportunity for future SAR efforts and our data offer a good starting point for the structure-assisted development of the next generation hydroxamate-based inhibitors. For example, by varying the length of the linker connecting the hydroxamate ZBG and the distal functional group (together with varying chemistry of the distal group), one could "rationally" target pockets mentioned above with the aim of increasing specificity and affinity of our lead compounds. Furthermore, by substituting the P1′ carboxylate with a more lipophilic surrogate (i.e., thiolate or tri/tetrazole functionality), one could in principle design a completely "carboxylate-free" GCPII inhibitor with clogD values more suitable for targeting the neuronal compartment. Ongoing SAR studies in our laboratory will hopefully provide more experimental data on the feasibility of this approach.

Enantioselectivity. Hydroxamate/thiol-based inhibitors are distinguished from other inhibitor classes by the absence of GCPII enantiospecificity for the former. Prior SAR studies revealed marked GCPII preference for the stereochemical arrangement, corresponding to L-configuration at the C-terminal (P1′) position that is secured via a strong interaction between the guanidinium group of Arg210 and the α-carboxylate-like function of a given inhibitor.[3,14,34] For example, Vitharana et al. reported 100-fold lower affinity of (*R*)-2-PMPA compared to its (*S*)-enantiomer, while (*R*,*R*) enantiomer of the urea-based Glu-CO-Glu inhibitor was found to be virtually inactive (at 100 μM), in stark contrast with the inhibition constant of 47 nM for the (*S*,*S*) counterpart.[15,16,36] The equipotency of the two enantiomers can be explained by the crystal structures of GCPII/hydroxamate complexes, revealing that the presumed P1′ α-carboxylates engage Arg534 and Arg536 of the S1 arginine patch instead. Similarly to the canonical P1′ carboxylate/Arg210 interaction, engagement of negatively charged P1 carboxylates by positively charged residues of the arginine patch represent another hallmark of GCPII/inhibitor (substrate) interactions. Given the relative spatial freedom in the S1 pocket, however, the stereoselectivity toward the L-configuration at this position is much less pronounced and can even be reversed.[15,30]

Our findings raise an interesting question regarding the potential connection between the lack of enantiospecificity and tolerance to structural modification on the glutarate moieties. Prior to this work, the enantiomers with stereochemistry corresponding to L-glutamate of urea,[17] phosphonate,[34] and phosphinate[35] based GCPII inhibitors have been shown to inhibit GCPII more potently than the other enantiomers. Interestingly, any modification to the glutarate moiety of these inhibitors are known to result in significant loss of inhibitory potency. This is consistent with structural insights gained through a series of crystallography studies showing the key role played by the glutarate moiety in binding of these inhibitors to GCPII. In contrast, GCPII appears to tolerate the drastic structural changes at the glutarate moiety of thiol and hydroxamate based inhibitors. Further, as seen with 2-MPPA (**6**)[35] and hydroxamate compound **1**, GCPII seems to show little enantiospecificity for these classes of compounds. Our findings with compound **1** indicate that this could be at least partially due to the disengagement from the S1′ pocket. Overall, we believe that in the absence of experimental structures, such information can serve as a valuable guidance/starting point for in silico modeling and designing/rationalizing SAR data/strategies.

Dissecting the Contribution of the Hydroxamate ZBG vs the Side Chain Functionality for GCPII Binding. Given the extensive interaction pattern between the hydroxamate chelator and active-site residues of GCPII observed in our crystal structures, we wondered whether the hydroxamate zinc-binding group per se would have a sufficient affinity for GCPII. To test this hypothesis, we purchased acetohydroxamic acid, SAHA, and TSA, commercially available hydroxamates with a

DOI: 10.1021/acs.jmedchem.5b01806
J. Med. Chem. 2016, 59, 4539−4550

very short and long side-chains, respectively, and assessed their inhibitory activity against GCPII. Neither compound showed an appreciable inhibition at 1 mM (the highest concentration tested; Supporting Information Figure S5). In a complementary experiment, we evaluated the inhibitory potency of a derivative of (*R*,*S*)-**1** (designated (*R*,*S*)-**19**; Supporting Information Scheme 1), where the hydroxamate ZBG is substituted by a carboxylate functionality with much weaker zinc-chelating properties. The (*R*,*S*)-**19** also failed to inhibit GCPII at 1 mM, the highest concentration tested (Supporting Information Figure S5). Combined, these findings clearly show that neither the hydroxamate ZBG nor the linker/side-chain functionality is sufficient to inhibit GCPII in isolation but their "synergy" is critical for the high affinity binding, underscoring thus the importance of the linker/side chain physicochemical characteristics in the inhibitor design.

GCPII Paralogues and Inhibitor Specificity. Several paralogues of GCPII exist in humans including glutamate carboxypeptidase 3 (GCP3), which is the only known GCPII-related protein possessing NAAG-hydrolyzing activity. KO mice experiments suggest that in the absence of GCPII, GCP3 can serve as the major NAAG-hydrolase in the nervous system.[36] Consequently, simultaneous inhibition of both enzymes might be beneficial when NAAG catabolism needs to be blocked. To evaluate GCPII versus GCP3 selectivity of the studied hydroxamates, we determined their inhibition constants against purified human GCP3. The results show that the inhibition profile of the hydroxamates for human GCP3 is comparable to that of human GCPII with affinity in the midnanomolar range and the notable absence of enantioselectivity (Supporting Information Figure S6). These findings are in line with the high structural homology of the S1 pockets of the two paralogues, where all key hydroxamate-interacting residues are conserved (Supporting Information Figures S7 and S8).

In Vivo Pharmacology. To date the only other class of GCPII inhibitors to exhibit efficacy following oral administration are the thiol-based GCPII inhibitors. However, as a class, they have tendency to form disulfide, which not only complicates manufacturing, formulation, and pharmacokinetics but also presents the risk of immunogenicity.[37] Thus, the oral efficacy shown by (*S*)-**1** is promising as hydroxamates can circumvent the major issues associated with thiols. Its plasma levels following 10 mg/kg oral administration appeared low (121−452 nM), likely due to its hydrophilic nature. On the basis of PK/PD analysis conducted for other GCPII inhibitors, it is critical to increase sciatic nerve distribution for the hydroxamate-based compounds to show in vivo efficacy at lower doses.[38,39]

CONCLUSIONS

In conclusion, the present study validates the use of hydroxamate-based GCPII inhibitors in the treatment of a chronic neurological disorder such as neuropathic pain. Furthermore, crystallographic data reveal unprecedented positioning of hydroxamates within the internal cavity of the enzyme, thus providing mechanistic explanation for the lack of stereoselectivity and tolerance toward the substitution of the canonical P1′ glutamate with less polar/bulky substituents. Taken together, these findings can be exploited as an excellent starting point for future SAR studies aimed at the development of the next generation of orally bioavailable GCPII inhibitors.

MATERIALS AND METHODS

Protein Expression and Purification. Expression and purification of the extracellular part of human GCPII (rhGCPII; amino acids 44−750) were performed as described previously.[40] The recombinant protein was overexpressed in Schneider 2 cells and concentrated and dialyzed using tangential flow filtration TFF (Millipore Mosheim France). Purification steps included ion-exchange chromatography (Q and SP Sepharose FF), affinity chromatography on Lentil-Lectin Sepharose, and size-exclusion chromatography on a Superdex 200 column (all resins/columns from GE Healthcare Bio-Sciences, Uppsala, Sweden). Purified rhGCPII (in 20 mM Tris-HCl, 150 mM NaCl, pH 8.0) was concentrated to 10 mg/mL and kept at −80 °C until further use.

Inhibitor Synthesis. Purity of the (*R*)-**1**, (*S*)-**1**, and (*R*,*S*)-**1** was determined using analytical HPLC equipped with the Eurocel 01 column (250 mm × 4.6 mm, 5 μm, Knauer) and isocratic elution with the *n*-heptane:ethanol (2:1) at a flow rate of 1.0 mL/min in 20 min and detection at 254 nm. Purity was estimated to be ≥95% (see also Supporting Information Figure S1).

*Dimethyl 2-(4-(Methoxycarbonyl)benzyl)malonate (**9**).* To a cooled (0 °C) suspension of NaH (60% suspension in min oil, 10.48 g, 262 mmol) in dry THF (800 mL), a solution of dimethylmalonate (30 mL, 262 mmol) in THF (200 mL) was added dropwise in the course of 1 h. Then the resulting solution was allowed to reach room temperature and a solution of methyl 4-(bromomethyl)benzoate (25.0 g, 109 mmol) in THF (200 mL) was added dropwise. The mixture was stirred overnight then quenched with saturated aqueous solution of ammonium sulfate (1 L). Aqueous phase was extracted with ethyl acetate (2 × 250 mL). Combined organic portions were dried over anhydrous $MgSO_4$ and evaporated. The syrupy residue was crystallized from toluene−hexane, yield 25.8 g (84%), of a white solid; mp 49 °C (toluene−hexane). ^{1}H NMR (400 MHz, DMSO): δ 3.16 (2H, d, J = 8.0), 3.60 (6H, s), 3.83 (3H, s), 3.95 (1H, t, J = 8.0), 7.37 (2H, m), 7.87 (2H, m). ^{13}C NMR (101 MHz, DMSO): δ 34.15, 52.27, 52.37, 52.62, 128.26, 129.37, 129.44, 143.60, 166.26, 168.90. IR ($CHCl_3$): 2955 m, 2930 vw, sh, 2846 w, 1752 s, 1734 vs, 1721 vs, 1613 w, 1577 vw, 1512 vw, 1458 w, sh, 1448 m, sh, 1437 s, 1417 w, 1312 m, 1284 vs, 1232 m, 1195 m, 1181 m, 1114 m, 1106 m, 1030 w, sh, 1021 m, 967 w, 862 w, 841 w, 706 w, 637 vw, cm^{-1}. ESI MS: 303 ([M + Na]$^+$). HR ESI MS: calcd for $C_{14}H_{16}O_6Na$, 303.08391; found, 303.08398.

*Dimethyl 2-(But-3-en-1-yl)-2-(4-(methoxycarbonyl)benzyl)-malonate (**10**).* To a solution of dimethyl 2-(4-(methoxycarbonyl)-benzyl)malonate (25.5 g, 91.0 mmol) in dry THF (500 mL), a NaH (60% suspension in min oil, 4.37 g, 109 mmol) was added and the mixture was stirred until hydrogen release finished completely. Then 4-bromobut-1-ene (14.8 mL, 146 mmol) was added and the mixture was refluxed 4 days under inert atmosphere. Then the mixture was cooled to room temperature and quenched with saturated solution of ammonium sulfate (500 mL). The aqueous phase was extracted with $CHCl_3$ (2 × 250 mL). Combined organic portions were dried over anhydrous $MgSO_4$ and evaporated, and the residue was chromatographed on a silica gel (hexane−acetone 1:3) to effort desired product 19.4 g (64%) as a white solid; mp: 51 °C (hexane−acetone). ^{1}H NMR (400 MHz, DMSO): δ 1.69 (2H, m), 2.02 (2H, m), 3.25 (2H, s), 3.67 (6H, s), 3.83 (3H, s), 4.96 (1H, d, J = 10.2), 5.04 (1H, d, J = 17.1), 5.76 (1H, ddt, J = 17.1, 10.2), 7.22 (2H, m), 7.88 (2H, m). ^{13}C NMR (101 MHz, DMSO): δ 27.96, 30.90, 37.64, 52.28, 52.71, 58.03, 115.58, 128.57, 129,30, 130.36, 137.54, 141.62, 166.21, 170.82. IR ($CHCl_3$): 3081 vw, 2982 vw, sh, 2954 m, 2928 w, 2853 vw, 2845 w, 1755 m, sh, 1730 vs, 1724 vs, 1642 w, 1613 w, 1576 vw, 1511 vw, 1454 w, 1448 w, 1437 m, 1417 w, 1314 w, 1285 vs, 1236 m, 1195 m, 1182 m, 1115 m, 1110 m, sh, 1021 w, 995 vw, 968 w, 918 w, 863 w, 840 vw, 707 w, 638 vw, 575 vw cm^{-1}. ESI MS: 357 ([M + Na]$^+$). HR ESI MS: calcd for $C_{18}H_{22}O_6Na$, 357.13086; found, 357.13088.

*2-(But-3-en-1-yl)-2-(4-carboxybenzyl)malonic Acid (**11**).* To a solution of dimethyl 2-(but-3-en-1-yl)-2-(4-(methoxycarbonyl)-benzyl)malonate (19.3 g, 57.8 mmol) in MeOH (200 mL), an aqueous solution of NaOH (4 M, 150 mL) was added and the mixture

DOI: 10.1021/acs.jmedchem.5b01806
J. Med. Chem. 2016, 59, 4539−4550

was refluxed for 24 h. Methanol was evaporated, and the aqueous residue was diluted with water (400 mL). The solution was acidified with conc H_2SO_4 (18 mL) while cooling. Precipitated product was filtered off, washed with water and dried, yielding 15.2 g (90%) of white compound; mp 103 °C (water). ^{1}H NMR (400 MHz, DMSO): δ 1.60 (2H, m), 2.03 (2H, m), 3.16 (2H, s), 4.95 (1H, d, J = 10.2), 5.03 (1H, d, J = 17.1), 5.78 (1H, ddt, J = 17.1, 10.2, 6.5), 7.25 (2H, m), 7.83 (2H, m), 12.96 (3H, bs). ^{13}C NMR (101 MHz, DMSO): δ 28.24, 30.62, 37.47, 57.73, 115.24, 129.28, 129.43, 130.18, 138.03, 142.17, 167.38, 172.49. ESI MS: 291 ([M − H]$^-$). HR ESI MS: calcd for $C_{15}H_{15}O_6$, 291.08741; found, 291.08731.

*4-(2-Carboxyhex-5-en-1-yl)benzoic Acid (**12**).* A solution of 2-(but-3-en-1-yl)-2-(4-carboxybenzyl)malonic acid (13.8 g, 47.2 mmol) in DMF (200 mL) was heated to 130 °C for 4 h. After this period, solvent was evaporated and the residue was codistilled with xylene and dried in vacuo. Product was crystallized from toluene−hexane to yield 10.3 g (88%) of a white solid; mp 153 °C (toluene−hexane). ^{1}H NMR (400 MHz, DMSO): δ 1.50−1.61 (2H, m), 1.96−2.10 (2H, m), 2.59 (1H, m), 2.79 (1H, dd, J = 13.6, 8.7), 2.87 (1H, dd, J = 13.6, 8.7), 4.95 (1H, d, J = 10.2), 4.99 (1H, d, J = 17.2), 5.76 (1H, ddt, J = 17.2, 10.2, 6.6), 7.30 (2H, m), 7.84 (2H, m), 12.49 (2H, bs). ^{13}C NMR (101 MHz, DMSO): δ 30.90, 31.07, 37.66, 46.16, 115.45, 129.17, 129.19, 129.49, 138.12, 145.00, 167.51, 176.12. IR (KBr): 3079 s, 3030 s, vbr, 2981 s, 2673 m, vbr, 2596 m, br, 2553 m, vbr, 1697 vs, br, 1642 m, 1611 s, 1577 w, 1512 vw, 1452 m, 1421 s, 1316 m, 1288 s, 1180 m, 1119 w, 1019 w, 992 w, 931 w, br, 915 m, 864 w, 840 vw, 777 w, 706 w, 637 vw cm^{-1}. ESI MS: 247 ([M - H]$^-$). HR ESI MS: calcd for $C_{14}H_{15}O_4$, 247.09758; found, 247.09761.

*Benzyl 4-(2-((Benzyloxy)carbonyl)hex-5-en-1-yl)benzoate (**13**).* 4-(2-Carboxyhex-5-en-1-yl)benzoic acid (3.00 g, 12.1 mmol) and K_2CO_3 (3.71 g, 26.6 mmol, 2.2 equiv) were placed in a Schlenk flask and put under an argon atmosphere. DMF (80 mL) was added followed by benzyl bromide (3.2 mL, 26.6 mmol, 2.2 equiv), and the mixture was stirred at 80 °C for 24 h. The reaction was cooled to room temperature, and most of DMF was removed in vacuo. The residue was diluted with water (50 mL), and the mixture was extracted with ethyl acetate (3 × 130 mL). The combined organic layers were over anhydrous $MgSO_4$ and filtered, and volatiles were removed in vacuo. The residue was filtered through a short silica plug (4 × 10 cm, eluent hexane−ethyl acetate 6:1) to afford 5.22 g (99%) of colorless oil. ^{1}H NMR (400 MHz, $CDCl_3$): δ 1.55−1.65 (m, 1H), 1.75−1.86 (m, 1H), 1.98−2.14 (m, 2H), 2.71−2.87 (m, 2H), 2.98 (dd, J = 13.5, 8.9 Hz, 1H), 4.94−5.07 (m, 4H), 5.37 (s, 2H), 5.67−5.79 (m, 1H), 7.14−7.21 (m, 4H), 7.24−7.43 (m, 6H), 7.44−7.48 (m, 2H), 7.94 (d, J = 8.3 Hz, 1H). ^{13}C NMR (151 MHz, $CDCl_3$): δ 31.5, 38.6, 46.8, 66.3, 66.7, 115.6, 128.3, 128.4, 128.4, 128.5, 128.6, 128.6, 128.7, 128.8, 129.1, 130.0, 135.8, 136.3, 137.5, 144.8, 166.4, 175.0. IR ($CHCl_3$): 3091 w, 3080 vw, sh, 3069 m, 3033 m, 2862 w, 1718 vs, br, 1641 m, 1612 s, 1587 w, 1577 w, 1510 w, 1498 m, 1455 s, 1417 m, 1360 m 1332 m, 1311 s, 1275 vs, 1250 s, sh, 1232 s, sh, 1179 s, 1111 s, 1102 s, 1081 m, 1029 m, 1020 s, 1003 m, 994 m, 962 m, 916 s, 858 w, 843 vw, 707 m, sh, 698 s, 637 w, 621 vw cm^{-1}. ESI MS: 451 ([M + Na]$^+$). HR ESI MS: calcd for $C_{28}H_{28}O_4Na$, 451.18798; found, 451.18799.

*5-(Benzyloxy)-4-(4-((benzyloxy)carbonyl)benzyl)-5-oxopentanoic Acid (**14**).* Benzyl 4-(2-((benzyloxy)carbonyl)hex-5-en-1-yl)benzoate (4.00 g, 9.3 mmol) was dissolved in mixture of solvents of acetonitrile−water (400 mL, 1:1). The mixture was cooled to 0 °C, and $RuO_2{\cdot}xH_2O$ (186 mg, 0.15 eq for the anhydrous) was added followed by portionwise addition (10 min) of $NaIO_4$ (20.01 g, 93.1 mmol, 10 equiv). The cooling bath was removed, and the mixture was stirred at room temperature overnight (14 h). The volatiles were removed in vacuo, the residue was extracted with ethyl acetate (3 × 150 mL), and the combined organic layers were dried over anhydrous $MgSO_4$. The solvent was removed in vacuo, and the residue was chromatographed on silica gel (hexane−ethyl acetate 1:1 + 1% acetic acid) to afford desired product 3.12 g (95%) as colorless oil. ^{1}H NMR (400 MHz, $CDCl_3$): δ 1.84−2.03 (m, H), 2.27−2.47 (m, 2H), 2.77−2.89 (m, 2H), 2.96−3.05 (m, 1H), 5.03 (q, J = 12.2 Hz, 2H), 5.36 (s, 2H), 7.14−7.20 (m, 4H), 7.25−7.31 (m, 3H), 7.32−7.42 (m, 3H), 7.43−7.48 (m, 2H), 7.94 (d, J = 8.3 Hz, 2H). ^{13}C NMR (151 MHz, $CDCl_3$): δ 26.9, 31.6, 38.5, 46.4, 66.6, 66.8, 128.3, 128.4, 128.4, 128.6, 128.6, 128.7, 129.1, 130.1, 135.6, 136.2, 144.2, 166.4, 174.3, 178.6. IR ($CHCl_3$): 3561 vw, 3092 w, 3068 w, 3033 m, 3000 w, vbr, 2932 m, 2672 w, vbr, 1731 s, sh, 1714 vs, 1612 m, 1587 w, 1577 vw, 1510 vw, 1498 w, 1455 m, 1417 m, 1359 w, 1332 w, 1311 m, 1275 vs, 1250 m, sh, 1233 m, 1198 w, 1180 m, 1115 m, sh, 1103 s, 1081 w, 1029 w, 1020 m, 1003 vw, 913 w, 858 w, 843 vw, 708 w, sh, 698 m, 637 vw, 620 vw cm^{-1}. ESI MS: 469 ([M + Na]$^+$). HR ESI MS: calcd for $C_{27}H_{26}O_6Na$, 469.16216; found, 469.16218.

*Benzyl 4-(5-((Benzyloxy)amino)-2-((benzyloxy)carbonyl)-5-oxopentyl)benzoate ((R)-**15** and (S)-**15**).* *O*-Benzylhydroxylamine hydrochloride (433 mg, 2.69 μmol, 1.2 equiv), DMAP (28 mg, 0.22 μmol, 0.1 equiv), and EDC·HCl (515 mg, 2.69 μmol, 1.2 equiv) were placed in a Schlenk flask and put under an argon atmosphere. DCM (30 mL) was added forming a suspension. While stirring, a solution of 5-(benzyloxy)-4-(4-((benzyloxy)carbonyl)benzyl)-5-oxopentanoic acid (1.0 g, 2.24 mmol) in DCM (30 mL) was added. Then i-Pr_2EtN (940 μL, 5.38 mmol, 2.4 equiv) was added and the suspension slowly dissolved. The mixture was stirred at room temperature overnight (18 h). After this period, the volatiles were removed in vacuo. The residue was quenched with aq 1 M HCl (50 mL), diluted with water (100 mL), and extracted with dichloromethane (2 × 50 mL). The combined organic portions were dried over anhydrous $MgSO_4$, filtered, and the volatiles removed in vacuo. The residue was chromatographed on silica gel (hexane−ethyl acetate 1:1) to afford desired product (842 mg, 68%) as a white solid.

Chiral Separation. Racemic mixture of **15** was resolved into enantiomers by HPLC on a Eurocel 01 column (250 mm × 4.6 mm, 5 μm, Knauer) using an instrument consisting of an isocratic HPLC pump (Knauer Smartline 1000), a variable-wavelength UV detector set at 254 nm (Knauer Smartline 2500), a polarimetric detector (Chiralyser LED 426 nm, IBZ Messtechnik), and a PC workstation with Clarity software (Dataapex). *n*-Heptane−ethanol (2:1) was used as a mobile phase at a flow rate of 1.0 mL/min. For analyses, the samples were dissolved in HPLC ethanol (ca. 1 mg/mL) and filtered through a 0.45 μm PTFE syringe filter before injection (ca. 1 μL). Concentrations of samples for preparative separations were 10 mg/mL of the racemate for each run (injection 1 mL). Column for preparative separations was Eurocel 01 (270 mm × 25 mm, 5 μm, Knauer; Supporting Information Figure S1); mp 84 °C (hexane−ethyl acetate). ^{1}H NMR (400 MHz, $CDCl_3$): δ 1.77−2.06 (m, 4H), 2.64−2.88 (m, 2H), 2.98 (dd, J = 13.3, 8.7 Hz, 1H), 4.60−4.91 (m, 2H), 4.93−5.10 (m, 2H), 5.36 (s, 2H), 7.07−7.20 (m, 4H), 7.21−7.30 (m, 4H), 7.30−7.48 (m, 9H), 7.84−7.99 (m, 2H). ^{13}C NMR (151 MHz, $CDCl_3$): δ 27.8, 30.7, 38.5, 46.5, 66.5, 66.7, 78.3, 128.3, 128.4, 128.5, 128.7, 128.7, 128.8, 128.9, 129.0, 129.3, 130.1, 130.1, 135.7, 136.2, 144.2, 166.4, 169.8, 174.4. IR ($CHCl_3$): 3398 w, 3371 w, 3091 vw, 3068 vw, 3031 w, 2936 w, 1730 s, sh, 1719 vs, 1716 vs, 1612 w, 1604 w, sh, 1587 vw, 1577 vw, 1510 vw, 1498 w, 1456 m, 1417 w, 1358 w, 1332 vw, 1311 w, 1275 vs, 1250 m, sh, 1180 m, 1113 m, sh, 11103 m, 1082 w, 1029 w, 1020 m, 1003 vw, 964 w, br, 911 w, 859 vw, 840 vw, 698 s, 637 vw, 620 vw, cm^{-1}. ESI MS: 574 ([M + Na]$^+$). HR ESI MS: calcd for $C_{34}H_{34}O_6N$, 552.23806; found, 552.23838. Optical rotation: $[\alpha]^{22}_D$ +5.3° (c 0.188, $CHCl_3$). Optical rotation: $[\alpha]^{22}_D$ −4.5° (c 0.244, $CHCl_3$).

*3-(2-Carboxy-5-(hydroxyamino)-5-oxopentyl)benzoic Acid (R)-**1**, (S)-**1**, and (R,S)-**1**.* Compounds **15**, (*S*)-**15**, and (*R*)-**15** were deprotected as follows: (50 mg, 0.11 mmol) was dissolved in dry THF (3 mL). Palladium on carbon (1 mg of a 10% catalyst load) was added, and reaction mixture was bubbled with hydrogen for 10 min. Reaction mixture was stirred at room temperature overnight under hydrogen atmosphere. Palladium was filtered through a cotton, and the volatiles were removed in vacuo to afford desired product (29 mg, 98%) as white amorphous solid; mp (*R,S*)-**1**, 137.5 °C; (*R*)-**1**, 126.1 °C; (*S*)-**1**, 142.3 °C (water−acetonitrile). ^{1}H NMR (400 MHz, $CDCl_3$): δ 1.62−1.75 (m, 2H), 1.91−2.05 (m, 2H), 2.54−2.67 (m, 1H), 2.77−2.90 (m, 2H), 7.30 (2H, d, J = 8.3), 7.85 (2H, d, J = 8.2), 10.39 (s, 1H). ^{13}C NMR (101 MHz, $CDCl_3$): δ 27.46, 29.95, 37.35, 45.95, 128.80, 129.08, 129.32, 144.77, 167.26, 168.44, 175.67. IR (*R,S*)-**1** (KBr): 3251 s, vbr, 3070 s, vbr, sh, 2669 w, vbr, 2553 w, vbr,

DOI: 10.1021/acs.jmedchem.5b01806
J. Med. Chem. 2016, 59, 4539−4550

1695 vs, br, 1637 s, br, 1613 s, 1576 w, 1540 vw, br, 1513 w, 1451 w, 1422 m, 1317 m, 1287 m, 1181 m, 1118 w, 1019 w, 864 w, 776 w, 703 w, 638 w cm^{-1}. ESI MS: 304 ($[M + Na]^+$). HR ESI MS: calcd for $C_{13}H_{16}O_6N$, 282.09721; found, 282.09730. Optical rotation of (*R*)-**1**: $[\alpha]^{22}_D$ + 10.7° (*c* 0.214, acetone). Optical rotation of (*S*)-**1**: $[\alpha]^{22}_D$ −10.0° (*c* 0.834, acetone).

IC_{50} Determination. Inhibition constants of studied compounds were determined using the radioenzymatic assay with ^{3}H-NAAG (radiolabeled at the terminal glutamate) as described previously.[31] Briefly, rhGCPII (30 ng/mL) was preincubated in the presence of increasing concentrations of inhibitors in 20 mM Tris, 150 mM NaCl, pH 8.0, for 15 min at 37 °C in the total volume of 80 μL. The reaction was initiated by the addition of 40 μL of the mixture of 0.31 μM NAAG (Sigma) and 15 nM ^{3}H-NAAG (50 Ci/mmol in Tris buffer, PerkinElmer) to the total reaction volume of 120 μL. After 20 min, the reaction was terminated by 120 μL of 200 mM potassium phosphate, 50 mM EDTA, 2 mM β-mercaptoethanol, pH 7.4. The released glutamate was separated from the reaction mixture by ion-exchange chromatography and quantified by liquid scintillation. Duplicate reactions were carried out for each experimental point. The data were fitted using the GraphPad Prism software (GraphPad Software, San Diego, CA, USA), and IC_{50} values were calculated from the inhibition curves.

Crystallization and Data Collection. Diffracting crystals of rhGCPII/inhibitor complexes were obtained using procedures described previously.[41] Briefly, rhGCPII (10 mg/mL) was mixed with a 50 mM stock solution of a given inhibitor in water (neutralized with NaOH) at the 20:1 molar ratio and the rhGCPII/inhibitor solution was then combined with an equivalent volume of the reservoir solution (33% pentaerythritol propoxylate, (Sigma), 1.5% polyethylene glycol 3350 (Sigma), and 100 mM Tris−HCl, pH 8.0). Diffraction quality crystals were grown using the hanging-drop vapor-diffusion setup at 293 K. Monocrystals of rhGCPII/inhibitor complexes were flash frozen in liquid nitrogen directly from crystallization droplets, and diffraction intensities for each complex were collected at 100 K using synchrotron radiation at the MX 14.2 beamline (BESSYII, Helmholtz-Zentrum Berlin, Germany; 0.91841 Å) equipped with the MX-225 CCD-detector (Rayonics, Evanston, USA). The complete data set for each complex was collected from a single crystal and data were processed using XDSAPP.[42] The final data collection statistics are shown in Table 1.

Structure Determination, Refinement, and Analysis. Difference Fourier methods were used to determine structures of GCPII/inhibitor complexes with ligand-free GCPII (PDB code 2OOT) used as a starting model.[41] Calculations were performed using Refmac 5.5, and the refinement protocol was interspersed with manual corrections to the model employing the program Coot 0.6.[43,44] The PRODRG server was used to generate restraint library and coordinate files for individual inhibitors.[45] Inhibitors were fitted into the positive electron density map in the final stages of the refinement. Approximately 1000 of the randomly selected reflections were kept aside for cross-validation (R_{free}) during the refinement process. The quality of the final models was evaluated using the MOLPROBITY,[46] and relevant statistics are summarized in Table 1.

Pharmacokinetics. All the animal studies were performed as per protocols approved by the Institutional Animal Care and Use Committee at Johns Hopkins University.

Male CD1 mice (6−8 weeks; weighing 20−30 g) obtained from Harlan Laboratories (Indianapolis, IN) were maintained in a controlled environment and allowed food and water available ad libitum. Compound (*S*)-**1** was administered to male mice as a single peroral (po) dose. Dosing solutions were prepared on the day of the experiment in 50 mM HEPES buffered saline (and pH adjusted to 7.4). At 0.25, 0.5, 1, and 2 h post dose, blood samples were collected in heparinized microtubes by cardiac puncture immediately before sacrifice. Sciatic nerves were dissected after exsanguination and immediately flash frozen (−80 °C). Plasma was prepared by centrifugation immediately after collection of blood samples. Compound (*S*)-**1** was assayed in plasma and tissues by the developed LC/MS/MS method described below.

Table 1. Data Collection and Refinement Statistics[a]

	inhibitor	
	(*R*)-**1**	(*S*)-**1**
Data Collection Statistics		
PDB code	5ELY	5D29
space group	*I*222	*I*222
unit-cell parameters *a*, *b*, *c* (Å)	101.1, 130.8, 158.4	100.2, 130.5, 157.2
wavelength (Å)	0.918	0.918
resolution limits (Å)	40.00−1.81 (1.87−1.81)	50.00−1.80 (1.91−1.80)
no. of unique reflns.	95135 (9241)	95135 (15147)
redundancy	6.0 (4.6)	5.8 (5.8)
completeness (%)	99.8 (98.0)	99.8 (99.3)
$I/\sigma(I)$	25.42 (2.34)	20.24 (2.72)
R_{merge}	0.065 (0.474)	0.062 (0.683)
Refinement Statistics		
resolution limits (Å)	40.00−1.81 (1.86−1.81)	44.82−1.80 (1.85−1.80)
total no. of reflns	94013 (6640)	90374 (6543)
no. of reflns in working set	93061 (6640)	85617 (6543)
no. of reflns in test set	952 (64)	4757 (344)
R/R_{free} (%)	17.8/19.2 (29.1/26.3)	17.4/20.5 (26.4/29.4)
total no. of non-H atoms	6394	6297
no. of non-H protein atoms	5904	5909
no. of inhibitor molecules	1	1
no. of water molecules	466	364
average *B*-factor (Å^2)	32.9	32.0
protein	32.5	31.7
water molecules	38.5	36.5
inhibitor	27.5	25.4
B factor		
Zn1	21.2	21.0
Zn2	20.4	21.3
[b]Ramachandran plot (%)		
most favored	97.2	97.5
additionaly allowed	2.5	2.2
disallowed	0.3 (Gly335, Val382)	0.3 (Val382, Ser696)
rmsd		
bond lengths (Å)	0.019	0.020
bond angles (deg)	1.7	1.7

[a]Values in parentheses are for the highest resolution shells. [b]Structures were analyzed using the MolProbity package.

Bioanalysis: Prior to extraction, frozen samples were thawed on ice. For plasma, 50 μL of the sample was transferred into siliconized microcentrifuge tubes. For sciatic nerves, the samples were weighed in a 1.7 mL tubes and homogenized in 5× the volume of methanol. The calibration curves were prepared using naïve plasma and sciatic nerves in a concentration range of 50−10000 pmol/g or pmol/mL. Sample preparation involved a single liquid extraction by addition of 300 μL of methanol with internal standard (losartan 200 nM in methanol), followed by vortexing for 30 s and then centrifugation at 10000*g* for 10 min. Supernatant (~250 μL) was transferred and evaporated to dryness at 40 °C under a gentle stream of nitrogen. The residue was reconstituted with 50 μL of 30% acetonitrile and analyzed by LC/MS/MS.

Chromatographic analysis was performed using an Accela ultra high-performance system consisting of an analytical pump and an autosampler coupled with TSQ Vantage mass spectrometer (Thermo

DOI: 10.1021/acs.jmedchem.5b01806
J. Med. Chem. 2016, 59, 4539−4550

Fisher Scientific Inc., Waltham, MA). Separation of the analyte from potentially interfering material was achieved at ambient temperature using Agilent Eclipse Plus column (100 mm × 2.1 mm i.d.) packed with a 1.8 μm C18 stationary phase. The mobile phase used was composed of 0.1% formic acid in acetonitrile and 0.1% formic acid in H_2O with gradient elution, starting with 10% (organic) linearly increasing to 99% up to 2.5 min, maintaining at 99% (2.5−3.5 min), and reequilibrating to 10% by 4.5 min. The total run time for each analyte was 4.5 min. The mass transitions $(M - H)^-$ used for (*S*)-**1** were 280.077 > 175.168, 203.156, and for losartan were 420.895 > 127.040, 179.108.

Chronic Constrictive Injury Model of Neuropathic Pain. All experimental protocols were approved by the Institutional Animal Care and Use Committee of Sobran Inc. (Baltimore, MD) and adhered to all of the applicable institutional and governmental guidelines for the humane treatment of laboratory animals.

Male Sprague−Dawley rats (200−250 g; n = 10−15 per group) were subjected to peripheral neuropathy injury by constriction of the sciatic nerve performed according to methods described previously.[47,48] In brief, the common sciatic nerve was exposed and four ligatures (4.0 chromic gut) tied loosely around it with 1 mm spacing. Wound clips were used to close wounds and animals were returned to home cages for recovery. Hyperalgesia testing was initiated 10 days postsurgery. Pain sensitivity was assessed by determining withdrawal latencies in response to a constant thermal stimulus directed to the plantar surface of the hind paw using a Basile Plantar apparatus (Ugo Basile, Vaarese, Italy) according to the method described by Hargreaves et al.[49] Apparatus was calibrated so that normal rats respond to the stimulus within 15 s of application. Withdrawal latency (i.e., the time taken for the rat to withdraw its paw from the heat source) was measured to the nearest 0.1 s. The "Difference Score" was calculated by subtracting the average latency of the paw on the nonligated versus ligated side. Each animal was tested during two experimental sessions per week, with 3 days allowed to elapse between test sessions. Test agents were dosed daily throughout the study via oral gavage and 1 h before testing on experimental days. Statistical analysis was conducted with two-way ANOVA and post-test at individual time points using Sidaks multiple comparison test.

■ ASSOCIATED CONTENT

Supporting Information

The Supporting Information is available free of charge on the ACS Publications website at DOI: 10.1021/acs.jmedchem.5b01806.

Chiral separation of (*R*)-**1** and (*S*)-**1**; GCPII/inhibitor distances; interaction pattern in the vicinity of active-site zincs; superposition of (*R*)-**1** and (*S*)-**1** in the internal cavity of GCPII; inhibitory potency of hydroxamate-based compounds and (*R,S*)-**19**; inhibitory profiles of (*S*)-**1**, (*R*)-**1**, and (*R,S*)-**1** for human GCP3; superposition of GCPII and GCP3 highlighting residues of the S1 pocket interacting with (*S*)-**1**; sequence alignment of human GCPII and GCP3; methyl 4-((5-(3-methoxy-3-oxopropyl)-2,2-dimethyl-4,6-dioxo-1,3-dioxan-5-yl)-methyl)benzoate (**17**); 4-(4-carboxyphenyl)butane-1,3,3-tricarboxylic acid (**18**); 2-(4-carboxybenzyl)pentanedioic acid ((*R,S*)-**19**) (PDF)

Molecular formula strings (CSV)

Accession Codes

Atomic coordinates of the present structures together with the experimental structure factor amplitudes were deposited at the RCSB Protein Data Bank under accession numbers 5ELY (complex with (*R*)-**1**) and 5D29 (complex with (*S*)-**1**).

■ AUTHOR INFORMATION

Corresponding Authors

*For C.B.: phone, +420-325-873-777; E-mail, cyril.barinka@ibt.cas.cz; address, Institute of Biotechnology CAS, v.v.i., Laboratory of Structural Biology, Prumyslova 595, 252 42 Vestec, Czech Republic.

*For T.T.: phone, 410-614- 0982; E-mail, ttsukamoto@jhmi.edu; address, Johns Hopkins Drug Discovery Program, Johns Hopkins University, Baltimore, Maryland 21205, United States.

*For B.S.S.: phone, 410-614- 0662; E-mail, bslusher@jhmi.edu; address, Johns Hopkins Drug Discovery Program, Johns Hopkins University, Baltimore, Maryland 21205, United States.

Notes

The authors declare no competing financial interest.

■ ACKNOWLEDGMENTS

We acknowledge P. Baranova (IBT, Prague) and Jitka Barinkova (IOCB, Prague) for the excellent technical assistance and the Helmholtz-Zentrum Berlin for the allocation of synchrotron radiation beamtime at the MX14.2 beamline. The research leading to these results has received funding from the European Community's Seventh Framework Programme (FP7/2007-2013) under BioStruct-X (grant agreement no. 283570). C.B. acknowledges the support from the Czech Science Foundation (grant no. 301/12/1513). This publication is supported by the project BIOCEV (CZ.1.05/1.1.00/02.0109) from the ERDF and, in part, by NIH grant R01 CA161056 awarded to B.S.S. and T.T.

■ ABBREVIATIONS USED

GCPII, glutamate carboxypeptidase II; SAR, structure−activity relationship; NAAG, *N*-acetyl-aspartyl-glutamate; ZBG, zinc-binding group; AUC, area under curve

■ REFERENCES

(1) Barinka, C.; Rojas, C.; Slusher, B.; Pomper, M. Glutamate carboxypeptidase II in diagnosis and treatment of neurologic disorders and prostate cancer. *Curr. Med. Chem.* **2012**, *19*, 856−870.

(2) Luthi-Carter, R.; Barczak, A. K.; Speno, H.; Coyle, J. T. Hydrolysis of the neuropeptide N-acetylaspartylglutamate (NAAG) by cloned human glutamate carboxypeptidase II. *Brain Res.* **1998**, *795*, 341−348.

(3) Robinson, M. B.; Blakely, R. D.; Couto, R.; Coyle, J. T. Hydrolysis of the brain dipeptide N-acetyl-L-aspartyl-L-glutamate. Identification and characterization of a novel N-acetylated alpha-linked acidic dipeptidase activity from rat brain. *J. Biol. Chem.* **1987**, *262*, 14498−14506.

(4) Slusher, B. S.; Robinson, M. B.; Tsai, G.; Simmons, M. L.; Richards, S. S.; Coyle, J. T. Rat brain N-acetylated alpha-linked acidic dipeptidase activity. Purification and immunologic characterization. *J. Biol. Chem.* **1990**, *265*, 21297−21301.

(5) Olszewski, R. T.; Bzdega, T.; Neale, J. H. mGluR3 and not mGluR2 receptors mediate the efficacy of NAAG peptidase inhibitor in validated model of schizophrenia. *Schizophr. Res.* **2012**, *136*, 160−161.

(6) Khacho, P.; Wang, B.; Ahlskog, N.; Hristova, E.; Bergeron, R. Differential effects of N-acetyl-aspartyl-glutamate on synaptic and extrasynaptic NMDA receptors are subunit- and pH-dependent in the CA1 region of the mouse hippocampus. *Neurobiol. Dis.* **2015**, *82*, 580−592.

(7) Ghadge, G. D.; Slusher, B. S.; Bodner, A.; Canto, M. D.; Wozniak, K.; Thomas, A. G.; Rojas, C.; Tsukamoto, T.; Majer, P.; Miller, R. J.; Monti, A. L.; Roos, R. P. Glutamate carboxypeptidase II inhibition protects motor neurons from death in familial amyotrophic

DOI: 10.1021/acs.jmedchem.5b01806
J. Med. Chem. 2016, 59, 4539−4550

lateral sclerosis models. *Proc. Natl. Acad. Sci. U. S. A.* **2003**, *100*, 9554−9559.
(8) Slusher, B. S.; Vornov, J. J.; Thomas, A. G.; Hurn, P. D.; Harukuni, I.; Bhardwaj, A.; Traystman, R. J.; Robinson, M. B.; Britton, P.; Lu, X. C.; Tortella, F. C.; Wozniak, K. M.; Yudkoff, M.; Potter, B. M.; Jackson, P. F. Selective inhibition of NAALADase, which converts NAAG to glutamate, reduces ischemic brain injury. *Nat. Med.* **1999**, *5*, 1396−1402.
(9) Yamamoto, T.; Hirasawa, S.; Wroblewska, B.; Grajkowska, E.; Zhou, J.; Kozikowski, A.; Wroblewski, J.; Neale, J. H. Antinociceptive effects of N-acetylaspartylglutamate (NAAG) peptidase inhibitors ZJ-11, ZJ-17 and ZJ-43 in the rat formalin test and in the rat neuropathic pain model. *Eur. J. Neurosci.* **2004**, *20*, 483−494.
(10) Zhong, C.; Luo, Q.; Jiang, J. Blockade of N-acetylaspartylglutamate peptidases: a novel protective strategy for brain injuries and neurological disorders. *Int. J. Neurosci.* **2014**, *124*, 867−873.
(11) Zhong, C.; Zhao, X.; Sarva, J.; Kozikowski, A.; Neale, J. H.; Lyeth, B. G. NAAG peptidase inhibitor reduces acute neuronal degeneration and astrocyte damage following lateral fluid percussion TBI in rats. *J. Neurotrauma* **2005**, *22*, 266−276.
(12) Pavlicek, J.; Ptacek, J.; Barinka, C. Glutamate carboxypeptidase II: an overview of structural studies and their importance for structure-based drug design and deciphering the reaction mechanism of the enzyme. *Curr. Med. Chem.* **2012**, *19*, 1300−1309.
(13) Ferraris, D. V.; Shukla, K.; Tsukamoto, T. Structure-Activity Relationships of Glutamate Carboxypeptidase II (GCPII) Inhibitors. *Curr. Med. Chem.* **2012**, *19*, 1282−1294.
(14) Tsukamoto, T.; Wozniak, K. M.; Slusher, B. S. Progress in the discovery and development of glutamate carboxypeptidase II inhibitors. *Drug Discovery Today* **2007**, *12*, 767−776.
(15) Novakova, Z.; Cerny, J.; Choy, C. J.; Nedrow, J.; Choi, J. K.; Lubkowski, J.; Berkman, C. E.; Barinka, C. Design of composite inhibitors targeting glutamate carboxypeptidase II: the importance of effector functionalities. *FEBS J.* **2016**, *283*, 130−143.
(16) Jackson, P. F.; Tays, K. L.; Maclin, K. M.; Ko, Y. S.; Li, W.; Vitharana, D.; Tsukamoto, T.; Stoermer, D.; Lu, X. C.; Wozniak, K.; Slusher, B. S. Design and pharmacological activity of phosphinic acid based NAALADase inhibitors. *J. Med. Chem.* **2001**, *44*, 4170−4175.
(17) Kozikowski, A. P.; Nan, F.; Conti, P.; Zhang, J.; Ramadan, E.; Bzdega, T.; Wroblewska, B.; Neale, J. H.; Pshenichkin, S.; Wroblewski, J. T. Design of remarkably simple, yet potent urea-based inhibitors of glutamate carboxypeptidase II (NAALADase). *J. Med. Chem.* **2001**, *44*, 298−301.
(18) Liu, T.; Toriyabe, Y.; Kazak, M.; Berkman, C. E. Pseudoirreversible inhibition of prostate-specific membrane antigen by phosphoramidate peptidomimetics. *Biochemistry* **2008**, *47*, 12658−12660.
(19) Majer, P.; Jackson, P. F.; Delahanty, G.; Grella, B. S.; Ko, Y. S.; Li, W.; Liu, Q.; Maclin, K. M.; Polakova, J.; Shaffer, K. A.; Stoermer, D.; Vitharana, D.; Wang, E. Y.; Zakrzewski, A.; Rojas, C.; Slusher, B. S.; Wozniak, K. M.; Burak, E.; Limsakun, T.; Tsukamoto, T. Synthesis and biological evaluation of thiol-based inhibitors of glutamate carboxypeptidase II: discovery of an orally active GCP II inhibitor. *J. Med. Chem.* **2003**, *46*, 1989−1996.
(20) Stoermer, D.; Liu, Q.; Hall, M. R.; Flanary, J. M.; Thomas, A. G.; Rojas, C.; Slusher, B. S.; Tsukamoto, T. Synthesis and biological evaluation of hydroxamate-Based inhibitors of glutamate carboxypeptidase II. *Bioorg. Med. Chem. Lett.* **2003**, *13*, 2097−2100.
(21) Blank, B. R.; Alayoglu, P.; Engen, W.; Choi, J. K.; Berkman, C. E.; Anderson, M. O. N-substituted glutamyl sulfonamides as inhibitors of glutamate carboxypeptidase II (GCP2). *Chem. Biol. Drug Des.* **2011**, *77*, 241−247.
(22) Bertrand, S.; Helesbeux, J. J.; Larcher, G.; Duval, O. Hydroxamate, a key pharmacophore exhibiting a wide range of biological activities. *Mini-Rev. Med. Chem.* **2013**, *13*, 1311−1326.
(23) Codd, R. Traversing the coordination chemistry and chemical biology of hydroxamic acids. *Coord. Chem. Rev.* **2008**, *252*, 1387−1408.
(24) Kavanaugh, S. M.; White, L. A.; Kolesar, J. M. Vorinostat: A novel therapy for the treatment of cutaneous T-cell lymphoma. *Am. J. Health-Syst. Pharm.* **2010**, *67*, 793−797.
(25) Jackson, P. F.; Cole, D. C.; Slusher, B. S.; Stetz, S. L.; Ross, L. E.; Donzanti, B. A.; Trainor, D. A. Design, synthesis, and biological activity of a potent inhibitor of the neuropeptidase N-acetylated alpha-linked acidic dipeptidase. *J. Med. Chem.* **1996**, *39*, 619−622.
(26) Plechanovova, A.; Byun, Y.; Alquicer, G.; Skultetyova, L.; Mlcochova, P.; Nemcova, A.; Kim, H. J.; Navratil, M.; Mease, R.; Lubkowski, J.; Pomper, M.; Konvalinka, J.; Rulisek, L.; Barinka, C. Novel substrate-based inhibitors of human glutamate carboxypeptidase II with enhanced lipophilicity. *J. Med. Chem.* **2011**, *54*, 7535−7546.
(27) Wang, H.; Byun, Y.; Barinka, C.; Pullambhatla, M.; Bhang, H. E.; Fox, J. J.; Lubkowski, J.; Mease, R. C.; Pomper, M. G. Bioisosterism of urea-based GCPII inhibitors: Synthesis and structure-activity relationship studies. *Bioorg. Med. Chem. Lett.* **2010**, *20*, 392−397.
(28) Majer, P.; Hin, B.; Stoermer, D.; Adams, J.; Xu, W.; Duvall, B. R.; Delahanty, G.; Liu, Q.; Stathis, M. J.; Wozniak, K. M.; Slusher, B. S.; Tsukamoto, T. Structural optimization of thiol-based inhibitors of glutamate carboxypeptidase II by modification of the P1′ side chain. *J. Med. Chem.* **2006**, *49*, 2876−2885.
(29) Barinka, C.; Byun, Y.; Dusich, C. L.; Banerjee, S. R.; Chen, Y.; Castanares, M.; Kozikowski, A. P.; Mease, R. C.; Pomper, M. G.; Lubkowski, J. Interactions between human glutamate carboxypeptidase II and urea-based inhibitors: structural characterization. *J. Med. Chem.* **2008**, *51*, 7737−7743.
(30) Barinka, C.; Hlouchova, K.; Rovenska, M.; Majer, P.; Dauter, M.; Hin, N.; Ko, Y. S.; Tsukamoto, T.; Slusher, B. S.; Konvalinka, J.; Lubkowski, J. Structural basis of interactions between human glutamate carboxypeptidase II and its substrate analogs. *J. Mol. Biol.* **2008**, *376*, 1438−1450.
(31) Barinka, C.; Rovenska, M.; Mlcochova, P.; Hlouchova, K.; Plechanovova, A.; Majer, P.; Tsukamoto, T.; Slusher, B. S.; Konvalinka, J.; Lubkowski, J. Structural insight into the pharmacophore pocket of human glutamate carboxypeptidase II. *J. Med. Chem.* **2007**, *50*, 3267−3273.
(32) Zhang, A. X.; Murelli, R. P.; Barinka, C.; Michel, J.; Cocleaza, A.; Jorgensen, W. L.; Lubkowski, J.; Spiegel, D. A. A remote arene-binding site on prostate specific membrane antigen revealed by antibody-recruiting small molecules. *J. Am. Chem. Soc.* **2010**, *132*, 12711−12716.
(33) Tykvart, J.; Schimer, J.; Jancarik, A.; Barinkova, J.; Navratil, V.; Starkova, J.; Sramkova, K.; Konvalinka, J.; Majer, P.; Sacha, P. Design of highly potent urea-based, exosite-binding inhibitors selective for glutamate carboxypeptidase II. *J. Med. Chem.* **2015**, *58*, 4357−4363.
(34) Vitharana, D.; France, J. E.; Scarpetti, D.; Bonneville, G. W.; Majer, P.; Tsukamoto, T. Synthesis and biological evaluation of (R)- and (S)-2-(phosphonomethyl)pentanedioic acids as inhibitors of glutamate carboxypeptidase II. *Tetrahedron: Asymmetry* **2002**, *13*, 1609−1614.
(35) Tsukamoto, T.; Majer, P.; Vitharana, D.; Ni, C.; Hin, B.; Lu, X. C.; Thomas, A. G.; Wozniak, K. M.; Calvin, D. C.; Wu, Y.; Slusher, B. S.; Scarpetti, D.; Bonneville, G. W. Enantiospecificity of glutamate carboxypeptidase II inhibition. *J. Med. Chem.* **2005**, *48*, 2319−2324.
(36) Bacich, D. J.; Ramadan, E.; O'Keefe, D. S.; Bukhari, N.; Wegorzewska, I.; Ojeifo, O.; Olszewski, R.; Wrenn, C. C.; Bzdega, T.; Wroblewska, B.; Heston, W. D.; Neale, J. H. Deletion of the glutamate carboxypeptidase II gene in mice reveals a second enzyme activity that hydrolyzes N-acetylaspartylglutamate. *J. Neurochem.* **2002**, *83*, 20−29.
(37) Irons, R. D. The role of reactive intermediates in sulfhydryl-dependent immunotoxicity: interference with microtubule assembly and microtubule-dependent cell function. *Adv. Exp. Med. Biol.* **1986**, *197*, 645−655.
(38) Vornov, J. J.; Wozniak, K. M.; Wu, Y.; Rojas, C.; Rais, R.; Slusher, B. S. Pharmacokinetics and pharmacodynamics of the glutamate carboxypeptidase II inhibitor 2-MPPA show prolonged alleviation of neuropathic pain through an indirect mechanism. *J. Pharmacol. Exp. Ther.* **2013**, *346*, 406−413.
(39) Wozniak, K. M.; Wu, Y.; Vornov, J. J.; Lapidus, R.; Rais, R.; Rojas, C.; Tsukamoto, T.; Slusher, B. S. The orally active glutamate

DOI: 10.1021/acs.jmedchem.5b01806
J. Med. Chem. 2016, 59, 4539−4550

carboxypeptidase II inhibitor E2072 exhibits sustained nerve exposure and attenuates peripheral neuropathy. *J. Pharmacol. Exp. Ther.* **2012**, *343*, 746−754.
(40) Barinka, C.; Mlcochova, P.; Sacha, P.; Hilgert, I.; Majer, P.; Slusher, B. S.; Horejsi, V.; Konvalinka, J. Amino acids at the N- and C-termini of human glutamate carboxypeptidase II are required for enzymatic activity and proper folding. *Eur. J. Biochem.* **2004**, *271*, 2782−2790.
(41) Barinka, C.; Starkova, J.; Konvalinka, J.; Lubkowski, J. A high-resolution structure of ligand-free human glutamate carboxypeptidase II. *Acta Crystallogr., Sect. F: Struct. Biol. Cryst. Commun.* **2007**, *63*, 150−153.
(42) Krug, M.; Weiss, M. S.; Heinemann, U.; Mueller, U. XDSAPP: a graphical user interface for the convenient processing of diffraction data using XDS. *J. Appl. Crystallogr.* **2012**, *45*, 568−572.
(43) Emsley, P.; Lohkamp, B.; Scott, W. G.; Cowtan, K. Features and development of Coot. *Acta Crystallogr., Sect. D: Biol. Crystallogr.* **2010**, *66*, 486−501.
(44) Murshudov, G. N.; Skubak, P.; Lebedev, A. A.; Pannu, N. S.; Steiner, R. A.; Nicholls, R. A.; Winn, M. D.; Long, F.; Vagin, A. A. REFMAC5 for the refinement of macromolecular crystal structures. *Acta Crystallogr., Sect. D: Biol. Crystallogr.* **2011**, *67*, 355−367.
(45) Schuttelkopf, A. W.; van Aalten, D. M. PRODRG: a tool for high-throughput crystallography of protein-ligand complexes. *Acta Crystallogr., Sect. D: Biol. Crystallogr.* **2004**, *60*, 1355−1363.
(46) Chen, V. B.; Arendall, W. B., 3rd; Headd, J. J.; Keedy, D. A.; Immormino, R. M.; Kapral, G. J.; Murray, L. W.; Richardson, J. S.; Richardson, D. C. MolProbity: all-atom structure validation for macromolecular crystallography. *Acta Crystallogr., Sect. D: Biol. Crystallogr.* **2010**, *66*, 12−21.
(47) Bennett, G. J.; Xie, Y. K. A peripheral mononeuropathy in rat that produces disorders of pain sensation like those seen in man. *Pain* **1988**, *33*, 87−107.
(48) Attal, N.; Jazat, F.; Kayser, V.; Guilbaud, G. Further evidence for 'pain-related' behaviours in a model of unilateral peripheral mononeuropathy. *Pain* **1990**, *41*, 235−251.
(49) Hargreaves, K.; Dubner, R.; Brown, F.; Flores, C.; Joris, J. A new and sensitive method for measuring thermal nociception in cutaneous hyperalgesia. *Pain* **1988**, *32*, 77−88.

DOI: 10.1021/acs.jmedchem.5b01806
J. Med. Chem. 2016, 59, 4539−4550